

Pre-Chirp-Domain Index Modulation for Full-Diversity Affine Frequency Division Multiplexing towards 6G

Guangyao Liu, Tianqi Mao, *Member, IEEE*, Zhenyu Xiao, *Senior Member, IEEE*, Ruiqi Liu, *Member, IEEE*, Miaowen Wen, *Senior Member, IEEE*,

Abstract—As a superior multicarrier technique utilizing chirp signals for high-mobility communications, affine frequency division multiplexing (AFDM) is envisioned to be a promising candidate for sixth-generation (6G) wireless networks. AFDM is based on the discrete affine Fourier transform (DAFT) with two adjustable parameters of the chirp signals, termed as the pre-chirp and post-chirp parameters, respectively. Whilst the post-chirp parameter complies with stringent constraints to combat time-frequency doubly selective channel fading, we show that the pre-chirp counterpart can be flexibly manipulated for an additional degree of freedom. Therefore, this paper proposes a novel AFDM scheme with the pre-chirp index modulation (PIM) philosophy (AFDM-PIM), which can implicitly convey extra information bits through dynamic pre-chirp parameter assignment, thus enhancing both spectral and energy efficiency. Specifically, we first demonstrate that the subcarrier orthogonality is still maintained by applying distinct pre-chirp parameters to various subcarriers in the AFDM modulation process. Inspired by this property, we allow each AFDM subcarrier to carry a unique pre-chirp signal according to the incoming bits. By such an arrangement, extra bits can be embedded into the index patterns of pre-chirp parameter assignment without additional energy consumption. We derive asymptotically tight upper bounds on the average bit error probability (BEP) of the proposed schemes with the maximum-likelihood detection, and validate that the proposed AFDM-PIM can achieve full diversity order under doubly dispersive channels. Based on the derived result, we further propose an optimal pre-chirp alphabet design to enhance the bit error rate (BER) performance via intelligent optimization algorithms. Simulation results demonstrate that the proposed AFDM-PIM outperforms the classical benchmarks.

Index Terms—Index modulation (IM), affine frequency division multiplexing (AFDM), discrete affine Fourier transform (DAFT), doubly dispersive channel.

I. INTRODUCTION

THE beyond fifth-generation (B5G) and sixth-generation (6G) wireless networks are envisioned to deliver ultra-reliable, high data rate, and low-latency communications for high-speed mobile scenarios, including low-earth-orbit (LEO)

This work was supported in part by the National Natural Science Foundation of China under Grants 62088101 and 62401054. Part of this work has been presented in IEEE IWCNC 2024 [1]. (*Corresponding authors: Zhenyu Xiao, Tianqi Mao.*)

G. Liu and Z. Xiao are with the School of Electronic and Information Engineering, Beihang University, Beijing 100191, China (liugy@buaa.edu.cn, xiaozy@buaa.edu.cn).

T. Mao is with State Key Laboratory of CNS/ATM, Beijing Institute of Technology, Beijing 100081, China, and is also with Beijing Institute of Technology (Zhuhai), Zhuhai 519088, China (e-mail: maotq@bit.edu.cn).

R. Liu is with the Wireless and Computing Research Institute, ZTE Corporation, Beijing 100029, China, and also with the State Key Laboratory of Mobile Network and Mobile Multimedia Technology, Shenzhen 518055, China (e-mail: richie.leo@zte.com.cn).

M. Wen is with the School of Electronic and Information Engineering, South China University of Technology, Guangzhou 510640, China (e-mail: eemwwen@scut.edu.cn).

satellite, high-mobility railway, unmanned aerial vehicles (UAV) and vehicle-to-vehicle (V2V) communications [2–5]. These scenarios inevitably suffer from severe Doppler shifts, which can cause time-frequency doubly selective channel fading (i.e., doubly dispersive channel) by involving the multi-path effects. This makes the existing modulation formats, like the main-stream orthogonal frequency division multiplexing (OFDM) in 4G/5G standards, no longer suitable for next-generation networks [6], which, thus, necessitates new waveform design with superior robustness to doubly dispersive channels. Consequently, it is crucial to develop new waveforms for next-generation communication networks to adapt to the doubly selective channel.

To date, several novel modulation schemes have been designed to combat time-frequency doubly selective fading, such as orthogonal time-frequency space (OTFS) [7–9] and orthogonal chirp-division multiplexing (OCDM) [10–12]. OTFS modulates information in the delay-Doppler (DD) domain using the inverse symplectic finite Fourier transform (ISFFT), which enables the transmission symbols to be multiplexed across the entire time-frequency domain [13–15]. OCDM utilizes a series of orthogonal chirp signals whose frequency varies with time to modulate information, which achieves better performance than the OFDM technique under doubly dispersive channels. However, the two-dimensional representation for the DD channel as in OTFS incurs significant pilot overhead, and the diversity gain OCDM can obtain is limited by specific channel profiles.

Against this background, affine frequency division multiplexing (AFDM) has been proposed based on the discrete affine Fourier transform (DAFT) [16], which can also combat the time-frequency doubly selective fading, and more importantly has less complexity to implement than OTFS since it requires only one-dimension transformation. DAFT is defined as one generalized discrete form of the discrete Fourier transform with a chirp-like basis specified by dual adjustable parameters, termed as pre-chirp and post-chirp parameters, respectively. In AFDM, data symbols are multiplexed onto chirp-like subcarriers through DAFT and inverse DAFT (IDAFT), which can separate the doubly dispersive channel into a sparse, quasi-static channel with a comprehensive DD channel representation by appropriately setting the chirp parameters. Therefore, the AFDM scheme achieves similar performance to OTFS, and demonstrates superior performance compared to the OFDM and OCDM schemes under the doubly selective channels [17].

There has been preliminary literature on AFDM [18–20]. A low-complexity embedded pilot-aided diagonal reconstruction (EPA-DR) channel estimation scheme was proposed in [18],

which calculates the AFDM effective channel matrix directly without estimating the three channel parameters, eliminating the severe inter-Doppler interference inherently. In [19], the authors investigated the AFDM-empowered sparse code multiple access (SCMA) systems to support massive connectivity in high-mobility environments. An AFDM-based integrated sensing and communications (ISAC) system was studied in [20], demonstrating that the AFDM-ISAC system can maintain excellent sensing performance even under significant Doppler shifts. The existing literature mostly explored the channel estimation, multiple access and ISAC issues under the classical AFDM architecture, whilst researches regarding further optimization/enhancement of the AFDM waveform are still at their infancies.

One promising research direction is to incorporate the index modulation philosophy for spectral and energy efficiency improvement [21, 22], which conveys energy-free bits through the activation patterns of transmit entities, e.g., subcarrier [23], time slots [24], pulse positioning [25], antennas [26], etc. In [27], Tao *et al.* presented an IM-assisted scheme, which conveys energy-free information bits through the activation patterns of the subsymbols in the DAFT-domain, verifying that index bits have stronger diversity protection than modulation bits. A multicarrier system using the activation patterns of AFDM chirp subcarriers as indices was developed in [28], which indicates the potential of IM-assisted AFDM technology in enhancing bit error rate (BER) and energy efficiency performance. However, existing research has concentrated on the post-chirp parameter in AFDM, with scant attention paid to the considerable flexibility and degrees of freedom (DoFs) that the pre-chirp parameter offers.

Inspired by this phenomenon, this paper proposes a novel AFDM scheme with the pre-chirp-domain index modulation (AFDM-PIM) to enhance spectral and energy efficiencies. Furthermore, performance evaluation of the proposed AFDM-PIM structure, including pairwise error probability (PEP) analysis and diversity analysis, is performed, and the numerical selection of the pre-chirp parameters is analyzed and optimized. The main contributions of this work are highlighted as follows:

- We demonstrate that the subcarrier orthogonality is maintained by applying distinct pre-chirp parameters to different subcarriers during the AFDM modulation process. Based on this property, each AFDM subcarrier is constructed with a unique pre-chirp signal corresponding to the incoming bits. This configuration allows for the embedding of additional bits into the index patterns of pre-chirp parameter assignment without additional energy consumption.
- We derive the input-output relationship of the proposed AFDM-PIM scheme in the DAFT domain, and the asymptotically tight upper bounds on the average bit error probability (BEP) with the maximum-likelihood (ML) detection based on the pairwise error probability (PEP) analysis. Furthermore, we validate that the proposed AFDM-PIM scheme can achieve full diversity order under doubly dispersive channels.
- We propose an optimal pre-chirp alphabet design to enhance the BER performance via particle swarm optimization (PSO) algorithm.

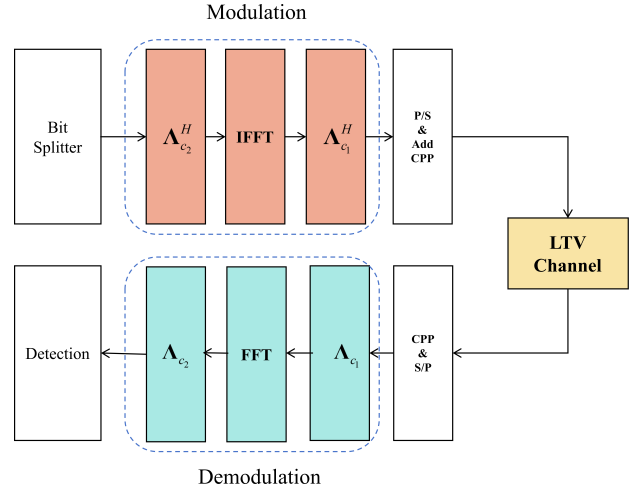


Fig. 1. The block diagram of AFDM system.

mization (PSO) algorithm.

- It is verified via computer simulations that the optimized pre-chirp parameter alphabet results in a much better BER performance than the heuristic selection of pre-chirp parameter values. Our results also demonstrate that the proposed AFDM-PIM scheme is superior to classical AFDM and IM-aided OFDM algorithms in terms of BER performance, which indicates the potential of AFDM-PIM in high-mobility communications scenarios.

The rest of the paper is organized as follows. In Section II, the AFDM system model is introduced. Afterwards, Section III describes the proposed AFDM-PIM scheme. The performance analysis of AFDM-PIM under doubly dispersive channels is presented in Section IV, including the PEP and diversity analysis. The pre-chirp parameter optimization is provided in Section V. Besides, the simulation results and discussions are provided in Section VI, and Section VII draws the conclusion.

Notation: In this paper, $\lfloor \cdot \rfloor$ denotes the integer floor operator. $|$ represents divisible. $s \sim \mathcal{CN}(0, \sigma^2)$ means that the random variable s follows a complex Gaussian distribution with zero mean and variance σ^2 . \bar{x} is the conjugate of complex numbers x . $\max(a, b)$ and $\min(a, b)$ represent the maximum and minimum values between a and b , respectively. $\binom{a}{b}$ denotes the number of ways to choose b elements from a set of a elements. $(\cdot)_N$ represents the modulo N operation. \mathbf{X}^T and \mathbf{X}^H stand for the transpose and Hermitian operations of \mathbf{X} , respectively. $\|\mathbf{X}\|_F$ represents the Frobenius norm of \mathbf{X} . $Q(\cdot)$ and $E(\cdot)$ denote the tail distribution function of the standard Gaussian distribution and the expectation operator, respectively. \mathbb{I} represents the set of irrational numbers. $\Re(x)$ denotes the operation that extracts the real component from the complex number x .

II. AFDM SYSTEM MODEL

The general system model of AFDM is presented in Fig. 1. For clarity, we provide a concise review of the fundamental concepts of AFDM [17]. The transmitted bit stream is initially mapped to a symbol vector, denoted as $\mathbf{x}_A = [x_A[0], x_A[1], \dots, x_A[N-1]]^T \in \mathbb{C}^{N \times 1}$, comprising N M -ary phase shift keying (PSK) symbols in the DAFT domain. The

resulting signals are then converted to time-domain representations with N -point IDAFT, formulated as

$$s_A[n] = \frac{1}{\sqrt{N}} \sum_{m=0}^{N-1} x_A[m] e^{i2\pi(c_1 n^2 + c_2 m^2 + \frac{mn}{N})}, \quad (1)$$

where $s_A[n]$ represents the time domain signal, and $m, n = 0, 1, \dots, N-1$. c_1 and c_2 are defined as the post-chirp and pre-chirp parameters of the DAFT, respectively.

Similarly to OFDM, AFDM also necessitates the insertion of prefix to address the multi-path problem. By leveraging the inherent periodicity characteristic of the DAFT, a chirp-periodic prefix (CPP) is incorporated to serve a function analogous to the cyclic prefix (CP) in OFDM, which is defined as

$$s_A[n] = s_A[N+n] e^{-i2\pi c_1(N^2+2Nn)}, \quad n = -L_{\text{CP}}, \dots, -1. \quad (2)$$

At the receiver, by discarding the CPP, the received AFDM signals in the DAFT domain can be expressed as

$$y_A[\bar{m}] = \sum_{p=1}^P h_p e^{i\frac{2\pi}{N}(Nc_1 d_p^2 - m d_p + Nc_2(m^2 - \bar{m}^2))} x_A[m] + w[\bar{m}], \quad (3)$$

$$\bar{m} = 0, 1, \dots, N-1,$$

where $w[\bar{m}] \sim \mathcal{CN}(0, N_0)$ represents the additive white Gaussian noise (AWGN); $h_p \sim \mathcal{CN}(0, 1/P)$ and d_p represent the channel coefficient and the non-negative integer delay normalized with the sampling period associated with the i -th path, respectively; \bar{m} and m are the indices in the DAFT domain. In matrix form, the received AFDM signals can be further expressed as

$$\mathbf{y}_A = \sum_{p=1}^P h_p \mathbf{A} \Gamma_{\text{CPP}_p} \Delta_{\nu_p} \mathbf{\Pi}^{d_p} \mathbf{A}^H \mathbf{x}_A + \mathbf{w}, \quad (4)$$

where $\Delta_{\nu_p} = \text{diag}(e^{-i2\pi\nu_p \cdot 0}, e^{-i2\pi\nu_p \cdot 1}, \dots, e^{-i2\pi\nu_p(N-1)})$ represents the Doppler effect, \mathbf{A} is the DAFT matrix, \mathbf{w} is the noise vector, $\mathbf{\Pi}$ represents the forward cyclic-shift matrix, written as

$$\mathbf{\Pi} = \begin{bmatrix} 0 & \cdots & 0 & 1 \\ 1 & \cdots & 0 & 0 \\ \vdots & \ddots & \ddots & \vdots \\ 0 & \cdots & 1 & 0 \end{bmatrix}_{N \times N}, \quad (5)$$

and Γ_{CPP_p} is an $N \times N$ diagonal matrix for CPP, written as

$$\Gamma_{\text{CPP}_p} = \text{diag} \left(\begin{cases} e^{-i2\pi c_1(N^2 - 2N(d_p - n))}, & n < d_p, \\ 1, & n \geq d_p, \end{cases} \right). \quad (6)$$

Upon receiving the signal \mathbf{y}_A , the ML detector can be employed for signal detection.

III. PROPOSED AFDM-PIM SCHEME

A. Orthogonality Analysis of AFDM Subcarriers

Following the modulation process of AFDM, (1) can also be expressed as

$$s_A[n] = \sum_{m=0}^{N-1} x_A[m] \phi_n(m), \quad n = 0, 1, \dots, N-1, \quad (7)$$

where $\phi_n(m)$ denotes the m -th chirp-like subcarrier, formulated as

$$\phi_n(m) = \frac{1}{\sqrt{N}} \cdot e^{i2\pi(c_1 n^2 + c_2 m^2 + \frac{mn}{N})}. \quad (8)$$

Below we propose Theorem 1 to present the superior flexibility of the c_2 assignment for different subcarriers.

Theorem 1: Applying distinct c_2 to different subcarriers in the AFDM modulation process will still preserve their orthogonality.

Proof: The inner product between two subcarriers of the AFDM, which utilize the same c_1 but distinct values of c_2 , designated as $\phi_n^{c_1, c_2, 1}(m)$ and $\phi_n^{c_1, c_2, 2}(m)$, can be calculated as

$$\begin{aligned} & \sum_{n=0}^{N-1} \phi_n^{c_1, c_2, 1}(m_1) \phi_n^{c_1, c_2, 2*}(m_2) \\ &= \frac{1}{N} e^{-i2\pi(c_{2,1} m_1^2 - c_{2,2} m_2^2)} \sum_{n=0}^{N-1} e^{-i\frac{2\pi}{N}(m_1 - m_2)n} \\ &= \frac{1}{N} e^{-i2\pi(c_{2,1} m_1^2 - c_{2,2} m_2^2)} \frac{1 - e^{-i2\pi N(\frac{m_1 - m_2}{N})}}{1 - e^{-i2\pi(\frac{m_1 - m_2}{N})}} \\ &= \begin{cases} 1, & m_1 = m_2, \\ 0, & \text{otherwise.} \end{cases} \end{aligned} \quad (9)$$

Therefore, it is evident that the orthogonality among AFDM subcarriers is not compromised when different values of c_2 are employed. \square

This insight provides a crucial foundation for our proposed AFDM-PIM scheme.

B. Transmitter

Inspired by Theorem 1, we propose the AFDM-PIM scheme, as shown in Fig. 2, which utilizes the flexibility of c_2 assignment to convey additional information bits. Consider the same AFDM symbol comprising N M -ary constellations symbols in the DAFT domain as in Section II.

At the transmitter, unlike classical AFDM, the N AFDM subcarriers are divided into G groups, with each group comprising $N_c = N/G$ chirp subcarriers. On the other hand, the total B information bits are split into G parallel streams of $b = B/G$ bits for each subcarrier group. Each b -bit stream is further segmented into b_1 data bits and b_2 index bits, i.e., $b = b_1 + b_2$. Within the g -th group ($1 \leq g \leq G$), the $b_1 = N_c \log_2(M)$ data bits are conveyed by N_c M -ary data symbols, denoted as $\mathbf{x}^g = [x^g[0], x^g[1], \dots, x^g[N_c - 1]] \in \mathbb{C}^{N_c \times 1}$. Meanwhile, each subcarrier is assigned with a unique c_2 value from one finite alphabet of λ legitimate c_2 realizations, i.e., $\mathcal{P}_c = \{c_2^{(1)}, c_2^{(2)}, \dots, c_2^{(\lambda)}\}$. Specifically, the pre-chirping pattern (PCP) of the c_2 values in the g -th group, denoted by $\mathbf{P}_{c_2}^g = [c_{2, N_c(g-1)}, c_{2, N_c(g-1)+1}, \dots, c_{2, N_c g-1}] \in \mathbb{C}^{N_c \times 1}$ is determined by the b_2 index bits according to the pre-defined relationship between the index-bit stream and the permutations of N_c elements from \mathcal{P}_c , where $c_{2,m} \in \mathcal{P}_c$ represents the pre-chirp parameter of the m -th subcarrier. $\mathbf{P}_{c_2} = [\mathbf{P}_{c_2}^1, \mathbf{P}_{c_2}^2, \dots, \mathbf{P}_{c_2}^G]$ represents the PCP for all groups (PCPG), and all possible PCPGs are combined into a set,

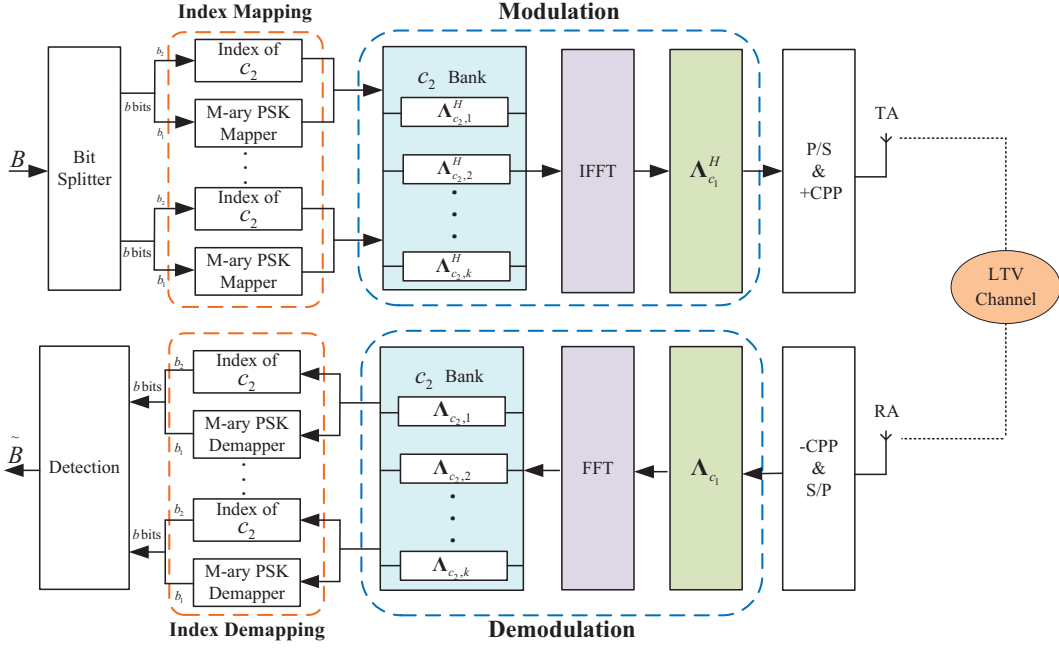


Fig. 2. Transceiver structure of the proposed AFDM-PIM scheme.

TABLE I
MAPPING RULE BETWEEN THE INDEX BITS AND THE PCPS IN THE CASE
OF $N_c = 4, \lambda = 4$.

Index bits	PCPs for Each Group			
	subcarrier 1	subcarrier 2	subcarrier 3	subcarrier 4
0000	$c_2^{(0)}$	$c_2^{(1)}$	$c_2^{(2)}$	$c_2^{(3)}$
0001	$c_2^{(0)}$	$c_2^{(1)}$	$c_2^{(3)}$	$c_2^{(2)}$
0010	$c_2^{(0)}$	$c_2^{(2)}$	$c_2^{(1)}$	$c_2^{(3)}$
0011	$c_2^{(0)}$	$c_2^{(2)}$	$c_2^{(3)}$	$c_2^{(1)}$
0100	$c_2^{(0)}$	$c_2^{(3)}$	$c_2^{(1)}$	$c_2^{(2)}$
0101	$c_2^{(0)}$	$c_2^{(3)}$	$c_2^{(2)}$	$c_2^{(1)}$
0110	$c_2^{(1)}$	$c_2^{(0)}$	$c_2^{(2)}$	$c_2^{(3)}$
0111	$c_2^{(1)}$	$c_2^{(0)}$	$c_2^{(3)}$	$c_2^{(2)}$
1000	$c_2^{(1)}$	$c_2^{(2)}$	$c_2^{(0)}$	$c_2^{(3)}$
1001	$c_2^{(1)}$	$c_2^{(2)}$	$c_2^{(3)}$	$c_2^{(0)}$
1010	$c_2^{(1)}$	$c_2^{(3)}$	$c_2^{(0)}$	$c_2^{(2)}$
1011	$c_2^{(1)}$	$c_2^{(3)}$	$c_2^{(2)}$	$c_2^{(0)}$
1100	$c_2^{(2)}$	$c_2^{(0)}$	$c_2^{(1)}$	$c_2^{(3)}$
1101	$c_2^{(2)}$	$c_2^{(0)}$	$c_2^{(3)}$	$c_2^{(1)}$
1110	$c_2^{(2)}$	$c_2^{(1)}$	$c_2^{(0)}$	$c_2^{(3)}$
1111	$c_2^{(2)}$	$c_2^{(1)}$	$c_2^{(3)}$	$c_2^{(0)}$

termed as \mathcal{S}_p . Table I exemplifies the mapping rule in the case of $N_c = 4, \lambda = 4$. Every b_2 index bits data corresponds to one row in Table I. Hence, aside from the classical PSK modulation, additional b_2 information bits can be implicitly conveyed by the indices of $\mathcal{P}_{c_2}^g$,

$$b_2 = \begin{cases} \lfloor \log_2(\mathcal{C}_{\lambda, N_c} N_c!) \rfloor, & \lambda \geq N_c, \\ \lfloor \log_2(\lambda!) \rfloor \frac{N_c}{\lambda}, & \lambda < N_c \text{ \& \ } \lambda \mid N_c, \\ \lfloor \log_2(\mathcal{C}_{\lambda, N_c} \lambda! \lambda^{(N_c - \lambda)}) \rfloor, & \text{otherwise,} \end{cases} \quad (10)$$

where $\mathcal{C}_{\lambda, N_c}$ is expressed as

$$\mathcal{C}_{\lambda, N_c} = \begin{pmatrix} \max(\lambda, N_c) \\ \min(\lambda, N_c) \end{pmatrix}. \quad (11)$$

After the mapping for all groups, the time-domain transmitted signals can be generated through N -point IDAFT operation, expressed as

$$s[n] = \frac{1}{\sqrt{N}} \sum_{m=0}^{N-1} x[m] e^{i2\pi(c_1 n^2 + c_{2,m} m^2 + nm/N)}. \quad (12)$$

The matrix form of (12) can be formulated as

$$\mathbf{s} = \mathbf{A}^H \mathbf{x} = \mathbf{\Lambda}_{c_1}^H \mathbf{F}^H \mathbf{\Lambda}_{c_2}^H \mathbf{x}, \quad (13)$$

where $\mathbf{x} = [\mathbf{x}^1, \mathbf{x}^2, \dots, \mathbf{x}^G]$, $\mathbf{\Lambda}_{c_2}$ and $\mathbf{\Lambda}_{c_1}$ represent the pre-chirp and post-chirp diagonal matrices, respectively, expressed as

$$\mathbf{\Lambda}_{c_2} = \text{diag} \left(e^{-i2\pi c_{2,k} n^2}, n, k = 0, 1, \dots, N-1 \right), \quad (14)$$

$$\mathbf{\Lambda}_{c_1} = \text{diag} \left(e^{-i2\pi c_1 n^2}, n = 0, 1, \dots, N-1 \right). \quad (15)$$

Besides, \mathbf{F} denotes the discrete Fourier transform (DFT) matrix with elements $\mathbf{F}(m, n) = e^{-i2\pi mn/N} / \sqrt{N}$, $m, n = 0, 1, \dots, N-1$.

Like classical AFDM, the proposed AFDM-PIM also requires the CPP to mitigate the effects of multi-path propagation effectively. Without loss of generality, the length of CPPs is assumed to be greater than the maximum channel delay spread.

C. Channel

Under high-mobility scenarios, the transmitted signals may experience time-frequency doubly dispersive channel

attributed to the severe Doppler shift and multi-path effects, which can be modeled as

$$h(\tau, \nu) = \sum_{p=1}^P h_p \delta(\tau - \tau_p) e^{-i2\pi\nu_p n}, \quad (16)$$

where P , ν_p , and τ_p represent the number of the paths, and the Doppler shift and delay of the p -th path, respectively. $h_p \sim \mathcal{CN}(0, 1/P)$ is the channel coefficient. The normalized delay and Doppler shift are given by $d_p = \tau_p \Delta f$ and $\alpha_p = NT\nu_p$, where Δf is the AFDM subcarrier spacing, T is the sampling interval and $T\Delta f = 1$. In this paper, we assume $\alpha_p \in [-\alpha_{\max}, \alpha_{\max}]$ and $d_p \in [0, d_{\max}]$, where α_{\max} and d_{\max} denote the maximum Doppler shift and maximum delay, respectively [27]. Besides, for simplicity, we mainly consider integer α_p values in this paper.

D. Receiver

The received time-domain signals after removing the CPP can be written as

$$r[n] = \sum_{p=1}^P h_p s[n - d_p] e^{-j2\pi\nu_p n} + w_r[n], \quad (17)$$

where $w_r[n] \sim \mathcal{CN}(0, N_0)$ is the complex additive Gaussian random noise. The matrix form of (17) is given by

$$\begin{aligned} \mathbf{r} &= \mathbf{H}\mathbf{s} + \mathbf{w} \\ &= \sum_{p=1}^P h_p \Gamma_{\text{CPP}_p} \Delta_{\nu_p} \Pi^{d_p} \mathbf{s} + \mathbf{w}_r, \end{aligned} \quad (18)$$

where $\mathbf{w}_r = [w_r[0], w_r[1], \dots, w_r[N-1]]$ denotes the $N \times 1$ noise vector in the time domain, Δ_{ν_p} represents the Doppler effect, Π is the forward cyclic-shift matrix, Π^{d_p} models the delay extension, and Γ_{CPP_p} is the effective CPP matrix, expressed as in Section II.

By applying the DAFT operation, the received DAFT-domain symbols are obtained as

$$y[\bar{m}] = \frac{1}{\sqrt{N}} \sum_{n=0}^{N-1} r[n] \cdot e^{-i2\pi(c_1 n^2 + c_2, \bar{m} \bar{m}^2 + n \bar{m} / N)}, \quad (19)$$

which can also expressed as

$$\begin{aligned} \mathbf{y} &= \mathbf{A}\mathbf{r} = \sum_{p=1}^P h_p \mathbf{A} \Gamma_{\text{CPP}_p} \Delta_{\nu_p} \Pi^{d_p} \mathbf{A}^H \mathbf{x} + \mathbf{A}\mathbf{w}_r \\ &= \mathbf{H}_{\text{eff}} \mathbf{x} + \mathbf{w}, \end{aligned} \quad (20)$$

where \mathbf{H}_{eff} is the effective channel matrix of the DAFT-domain and $\mathbf{w} = \mathbf{A}\mathbf{w}_r$.

Finally, the ML criterion can be employed for data detection, formulated as

$$\left(\hat{\mathbf{x}}, \hat{P}_{c_2} \right) = \arg \min_{\forall \mathbf{x}, P_{c_2}} \left\| \mathbf{y} - \hat{\mathbf{H}}_{\text{eff}} \mathbf{x} \right\|_{\text{F}}^2, \quad (21)$$

where $\hat{\mathbf{H}}_{\text{eff}}$ represents the estimated effective channel. The time-frequency doubly dispersive channel can be estimated through pilot-aided channel estimation algorithms [14, 18, 29]. This paper will not provide further elaboration on the subject for brevity.

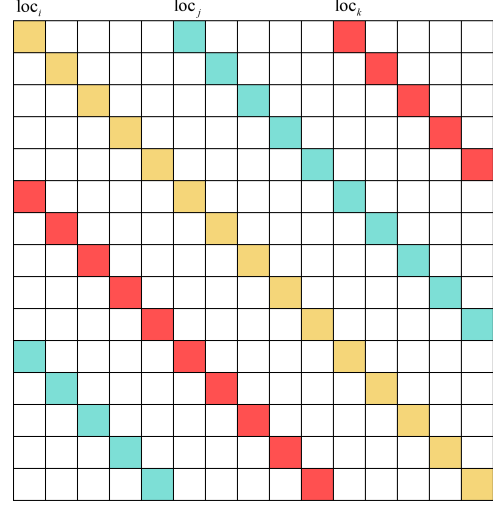


Fig. 3. Example of the structure with \mathbf{H}_i , \mathbf{H}_j and \mathbf{H}_k combined.

E. Input-Output Relation and Parameter Settings

Substituting (12) and (17) into (19), the input-output relation of AFDM-PIM can be obtained as

$$y[\bar{m}] = \frac{1}{N} \sum_{p=1}^P \sum_{m=0}^{N-1} h_p \xi_{(p, \bar{m}, m)} \eta_{(p, \bar{m}, m)} x[m] + w[\bar{m}], \quad (22)$$

where

$$\xi_{(p, \bar{m}, m)} = e^{i \frac{2\pi}{N} (Nc_{2,m} m^2 - Nc_{2,\bar{m}} \bar{m}^2 - md_p + Nc_1 d_p^2)}, \quad (23)$$

$$\begin{aligned} \eta_{(p, \bar{m}, m)} &= \sum_{n=0}^{N-1} e^{-i \frac{2\pi}{N} ((\bar{m}-m+\alpha_p+2Nc_1 d_p)n)} \\ &= \frac{e^{-i2\pi(\bar{m}-m+\alpha_p+2Nc_1 d_p)} - 1}{e^{-i \frac{2\pi}{N} (\bar{m}-m+\alpha_p+2Nc_1 d_p)} - 1}. \end{aligned} \quad (24)$$

In matrix representation, (22) can be rewritten as

$$\mathbf{y} = \sum_{p=1}^P h_p \mathbf{H}_p \mathbf{x} + \mathbf{w}, \quad (25)$$

where $\mathbf{H}_p = \mathbf{A} \Gamma_{\text{CPP}_p} \Delta_{\nu_p} \Pi^{d_p} \mathbf{A}^H$. According to (22)-(25), the element of \mathbf{H}_p can be obtained as

$$\begin{aligned} H_p[\bar{m}, m] &= \frac{1}{N} \xi_{(p, \bar{m}, m)} \eta_{(p, \bar{m}, m)} \\ &= \begin{cases} \xi_{(p, \bar{m}, m)}, & m = (\bar{m} + \text{loc}_p)_N, \\ 0, & \text{otherwise,} \end{cases} \end{aligned} \quad (26)$$

where $\text{loc}_p = (\alpha_p + 2Nc_1 d_p)_N$. Since the range of loc_p is $[-\alpha_{\max} + 2Nc_1 d_p, \alpha_{\max} + 2Nc_1 d_p]$, we define $\text{loc}_p \in \mathbb{K}_p$, where $\mathbb{K}_p = \{-\alpha_{\max} + 2Nc_1 d_p, \dots, \alpha_{\max} + 2Nc_1 d_p\}$.

It can be indicated from (26) that, concerning the two chirp parameters of AFDM-PIM, only the post-chirp parameter exerts an influence on the position of non-zero entries in the matrix \mathbf{H}_p determined by loc_p , which is independent of the pre-chirp parameter. Therefore, like classical AFDM, full diversity can be realized in the proposed AFDM-PIM under doubly dispersive channels by adjusting c_1 to avoid possible overlap between non-zero elements of \mathbf{H}_i and \mathbf{H}_j ($i \neq j$).

Specifically, it is imperative that the intersection between the corresponding ranges for loc_i and loc_j is empty, i.e.,

$$\mathbb{K}_i \cap \mathbb{K}_j = \emptyset. \quad (27)$$

Without loss of generality, we assume that $d_i \leq d_j$. Then the constraint from (27) can be transformed into

$$c_1 > \frac{2\alpha_{\max}}{2N(d_j - d_i)}. \quad (28)$$

Since minimum $(d_j - d_i)$ equals unity, it can be concluded that c_1 can be set as:

$$c_1 = \frac{2\alpha_{\max} + 1}{2N \min_{i,j}(d_j - d_i)} = \frac{2\alpha_{\max} + 1}{2N}. \quad (29)$$

Following the configuration in (29) and $(d_{\max} + 1)(2\alpha_{\max} + 1) \leq N$, the channel paths with different delay or Doppler shifts can be distinguished within the DAFT domain, as shown in Fig. 3. The rigorous diversity analysis will be provided in Section IV.

IV. PERFORMANCE ANALYSIS

In this section, we first derive the average bit error probability (ABEP) upper bounds for the proposed AFDM-PIM scheme, where the ML criterion is employed for detection. Then, we analyze the diversity order of AFDM-PIM.

A. Error Performance Analysis

To facilitate the analysis, the received DAFT-domain signal in (25) can be rewritten as

$$\mathbf{y} = \sum_{p=1}^P h_p \mathbf{H}_p \mathbf{x} + \mathbf{w} = \mathbf{\Phi}(\mathbf{x})\mathbf{h} + \mathbf{w}, \quad (30)$$

where $\mathbf{\Phi}(\mathbf{x}) = [\mathbf{H}_1 \mathbf{x}, \dots, \mathbf{H}_P \mathbf{x}] \in \mathbb{C}^{N \times P}$ and $\mathbf{h} = [h_1, h_2, \dots, h_P]^T \in \mathbb{C}^{P \times 1}$. The conditional PEP (CPEP) between $\mathbf{\Phi}(\mathbf{x})$ and the estimated $\hat{\mathbf{\Phi}}(\hat{\mathbf{x}})$ can be calculated as

$$\begin{aligned} \Pr([\mathbf{x}, \mathbf{\Phi}] \rightarrow [\hat{\mathbf{x}}, \hat{\mathbf{\Phi}}]|\mathbf{h}) \\ &= \Pr(\|\mathbf{y} - \hat{\mathbf{\Phi}}(\hat{\mathbf{x}})\mathbf{h}\|_{\mathbb{F}}^2 < \|\mathbf{y} - \mathbf{\Phi}(\mathbf{x})\mathbf{h}\|_{\mathbb{F}}^2) \\ &= \Pr(\chi > \|(\hat{\mathbf{\Phi}}(\hat{\mathbf{x}}) - \mathbf{\Phi}(\mathbf{x}))\mathbf{h}\|_{\mathbb{F}}^2). \end{aligned} \quad (31)$$

Here, $\chi = \mathbf{w}^H(\hat{\mathbf{\Phi}}(\hat{\mathbf{x}}) - \mathbf{\Phi}(\mathbf{x}))\mathbf{h} + \mathbf{h}^H(\hat{\mathbf{\Phi}}(\hat{\mathbf{x}}) - \mathbf{\Phi}(\mathbf{x}))^H \mathbf{w}$, which χ follows a Gaussian distribution with variance of $2N_0 \|(\hat{\mathbf{\Phi}}(\hat{\mathbf{x}}) - \mathbf{\Phi}(\mathbf{x}))\mathbf{h}\|_{\mathbb{F}}^2$. Therefore, the CPEP can be expressed as

$$\begin{aligned} \Pr([\mathbf{x}, \mathbf{\Phi}] \rightarrow [\hat{\mathbf{x}}, \hat{\mathbf{\Phi}}]|\mathbf{h}) \\ &= \Pr\left(\chi > \|(\hat{\mathbf{\Phi}}(\hat{\mathbf{x}}) - \mathbf{\Phi}(\mathbf{x}))\mathbf{h}\|_{\mathbb{F}}^2\right) \\ &= Q\left(\sqrt{\frac{\delta}{2N_0}}\right), \end{aligned} \quad (32)$$

where we define that $\delta = \|(\hat{\mathbf{\Phi}}(\hat{\mathbf{x}}) - \mathbf{\Phi}(\mathbf{x}))\mathbf{h}\|_{\mathbb{F}}^2 = \mathbf{h}^H \mathbf{\Psi} \mathbf{h}$ with $\mathbf{\Psi} = (\hat{\mathbf{\Phi}}(\hat{\mathbf{x}}) - \mathbf{\Phi}(\mathbf{x}))^H (\hat{\mathbf{\Phi}}(\hat{\mathbf{x}}) - \mathbf{\Phi}(\mathbf{x}))$. According to [30], $Q(\cdot)$ can be approximated as

$$Q(x) \cong \frac{1}{12}e^{-x^2/2} + \frac{1}{4}e^{-2x^2/3}. \quad (33)$$

Then, the CPEP can be rewritten as

$$\Pr([\mathbf{x}, \mathbf{\Phi}] \rightarrow [\hat{\mathbf{x}}, \hat{\mathbf{\Phi}}]|\mathbf{h}) \cong \frac{1}{12}e^{-\varsigma_1 \delta} + \frac{1}{4}e^{-\varsigma_2 \delta}, \quad (34)$$

where $\varsigma_1 = 1/(4N_0)$, $\varsigma_2 = 1/(3N_0)$. Afterwards, unconditional PEP (UPEP) can be calculated as

$$\begin{aligned} \Pr([\mathbf{x}, \mathbf{\Phi}] \rightarrow [\hat{\mathbf{x}}, \hat{\mathbf{\Phi}}]) \\ &= \mathbb{E}\left(\Pr([\mathbf{x}, \mathbf{\Phi}] \rightarrow [\hat{\mathbf{x}}, \hat{\mathbf{\Phi}}]|\mathbf{h})\right) \\ &\approx \int_0^{+\infty} \left(\frac{1}{12}e^{-q_1 \delta} + \frac{1}{4}e^{-q_2 \delta}\right) p_{\delta}(\delta) d\delta. \end{aligned} \quad (35)$$

By defining the moment-generating function (MGF) $M_{\delta}(s) = \mathbb{E}(e^{s\delta}) = \int_{-\infty}^{+\infty} e^{s\delta} p_{\delta}(\delta) d\delta$, we can calculate the UPEP of (35) as

$$\Pr([\mathbf{x}, \mathbf{\Phi}] \rightarrow [\hat{\mathbf{x}}, \hat{\mathbf{\Phi}}]) \approx \frac{1}{12}M_{\delta}(-q_1) + \frac{1}{4}M_{\delta}(-q_2). \quad (36)$$

Theorem 2 [31]: For the $N \times N$ Hermitian matrix \mathbf{Q} and $N \times 1$ zero mean complex vector \mathbf{v} , the characteristic function of the quadratic form $f = \mathbf{v}^H \mathbf{Q} \mathbf{v}$ can be expressed as

$$\varphi_f(t) = |\mathbf{I} - it\mathbf{L}\mathbf{Q}|^{-1} = \prod_{\iota=1}^{\kappa} \frac{1}{1 - it\lambda_{\iota}(\mathbf{L}\mathbf{Q})}, \quad (37)$$

where \mathbf{L} represents the complex covariance matrix of \mathbf{v} , $\lambda_{\iota}(\mathbf{L}\mathbf{Q})$ is the ι -th non-zero eigenvalue of matrix $\mathbf{L}\mathbf{Q}$ and κ denotes the number of the non-zero eigenvalues, i.e., the rank of matrix $\mathbf{L}\mathbf{Q}$. Then the MGF of f can be given by

$$M_f(s) = \varphi_f(-it) = \prod_{\iota=1}^{\kappa} \frac{1}{1 - s\lambda_{\iota}(\mathbf{L}\mathbf{Q})}. \quad (38)$$

Since \mathbf{h} is a zero mean complex vector and $\mathbf{\Psi}$ is a Hermitian matrix, according to Theorem 2, the UPEP in (36) can be further expressed as

$$\begin{aligned} \Pr([\mathbf{x}, \mathbf{\Phi}] \rightarrow [\hat{\mathbf{x}}, \hat{\mathbf{\Phi}}]) \\ &\approx \frac{1}{12} \prod_{\iota=1}^{\kappa} \frac{1}{1 + \frac{\lambda_{\iota}(\mathbf{L}\mathbf{\Psi})}{4N_0}} + \frac{1}{4} \prod_{\iota=1}^{\kappa} \frac{1}{1 + \frac{\lambda_{\iota}(\mathbf{L}\mathbf{\Psi})}{3N_0}} \\ &\approx \frac{1}{12} \prod_{\iota=1}^{\kappa} \frac{1}{1 + \frac{\lambda_{\iota}(\mathbf{\Psi})}{4PN_0}} + \frac{1}{4} \prod_{\iota=1}^{\kappa} \frac{1}{1 + \frac{\lambda_{\iota}(\mathbf{\Psi})}{3PN_0}}. \end{aligned} \quad (39)$$

Moreover, based on the UPEP obtained in (39), the ABEP upper bound for the proposed AFDM-PIM scheme can be calculated by (40), as shown at the top of the following page. Note that $\tau([\mathbf{x}, \mathbf{\Phi}] \rightarrow [\hat{\mathbf{x}}, \hat{\mathbf{\Phi}}])$ represents the number of error bits caused by the corresponding pairwise error event.

B. Diversity Analysis

At the high signal-to-noise ratio (SNR) region, the approximation of (39) can be simplified as

$$\begin{aligned} \Pr([\mathbf{x}, \mathbf{\Phi}] \rightarrow [\hat{\mathbf{x}}, \hat{\mathbf{\Phi}}]) \\ &\approx \left(\prod_{\iota=1}^{\kappa} \lambda_{\iota}(\mathbf{\Psi})\right)^{-1} \left(\frac{(4P)^{\kappa}}{12} + \frac{(3P)^{\kappa}}{4}\right) \text{SNR}^{-\kappa}, \end{aligned} \quad (41)$$

$$\text{Pr}_{\text{ABEP}} \leq \frac{1}{b^{2b}} \sum_{\mathbf{x}} \sum_{\hat{\mathbf{x}}} \sum_{\Phi} \sum_{\hat{\Phi}} \text{Pr}([\mathbf{x}, \Phi] \rightarrow [\hat{\mathbf{x}}, \hat{\Phi}]) \tau([\mathbf{x}, \Phi] \rightarrow [\hat{\mathbf{x}}, \hat{\Phi}]), \quad (40)$$

where SNR is defined as $1/N_0$. As a result, the diversity order μ of the proposed AFDM-PIM equals the minimum value of κ , i.e.,

$$\mu = \min \text{rank}(\Psi). \quad (42)$$

Note that the eigenvalues of Hermitian matrix Ψ can be calculated as the square of the singular values of $(\hat{\Phi}(\hat{\mathbf{x}}) - \Phi(\mathbf{x}))$. Consequently, it can be concluded that $\text{rank}(\Psi) = \text{rank}(\hat{\Phi}(\hat{\mathbf{x}}) - \Phi(\mathbf{x}))$ and the diversity order μ can be also expressed as

$$\mu = \min \text{rank}(\hat{\Phi}(\hat{\mathbf{x}}) - \Phi(\mathbf{x})). \quad (43)$$

Defining $\Phi(\delta) = \hat{\Phi}(\hat{\mathbf{x}}) - \Phi(\mathbf{x})$, the full diversity order analysis for AFDM-PIM can be transformed into the full rank analysis of $\Phi(\delta)$ as Theorem 3 below.

Theorem 3: The proposed AFDM-PIM scheme is capable of achieving the full diversity order if the following two conditions are met:

- **Condition 1:** the number of the paths satisfies

$$P \leq (d_{\max} + 1)(2\alpha_{\max} + 1) \leq N. \quad (44)$$

- **Condition 2:** The pre-chirp parameters in \mathcal{P}_c take as the irrational numbers.

Proof: See Appendix A. \square

V. PARAMETER OPTIMIZATION

In this section, we establish an optimization problem about the optimal c_2 alphabet design to enhance the BER performance, where the particle swarm optimization (PSO) algorithm is employed.

A. Problem Formulation

For tractable analysis, the pre-chirp alphabet design is investigated based on the optimal BER detector [32], i.e., the ML detector in (30), expressed as

$$(\tilde{\mathbf{x}}, \tilde{c}_2) = \arg \min_{\forall \mathbf{x}, c_2} \|\mathbf{y} - \Phi(\mathbf{x})\mathbf{h}\|_{\mathbb{F}}^2. \quad (45)$$

To achieve the optimal c_2 alphabet, the minimum Euclidean distance (MED) between different realizations of $\Phi(\mathbf{x})$ should be maximized. Specifically, the Euclidean distance between two realizations of $\Phi(\mathbf{x})$ can be formulated as

$$O_{k,j}(\mathcal{P}_c) = \sum_{\mathbf{x}' \neq \mathbf{x}} \sum_{r=1}^{\mathcal{R}} \left\| (\Phi_k^r(\mathbf{x}') - \Phi_j^r(\mathbf{x})) \right\|_{\mathbb{F}}^2, \quad (46)$$

where j, k represent the indices of \mathcal{S}_p , and the PCPGs corresponds j, k are expressed as $\text{P}_{c_2}^{(j)} = [c_{2,1}, c_{2,2}, \dots, c_{2,N}]$ and $\text{P}_{c_2}^{(k)} = [c'_{2,1}, c'_{2,2}, \dots, c'_{2,N}]$, respectively. Besides, r is the index of delay and Doppler selection. Specifically, each r corresponds to a specific combination of P paths with different delays and Doppler shifts. under doubly dispersive channel with a maximum delay d_{\max} and normalized Doppler shift of α_{\max} , and the maximum value of r is $\mathcal{R} = \binom{P_{\max}}{P}$, where $P_{\max} = (d_{\max} + 1)(2\alpha_{\max} + 1)$.

Besides, according to (14) and Theorem 3, it can be known that c_2 is an irrational number with a principal value range of $[0, 1]$. Afterwards, to enhance the BER performance of the proposed AFDM-PIM, we formulate the following problem to maximize the MED with optimal c_2 alphabet design:

$$\max_{\mathcal{P}_c} \min_{k,j \in [1, 2^{b_2}]} O_{k,j}(\mathcal{P}_c) \quad (47a)$$

$$\text{s.t. } j \neq k, \quad (47b)$$

$$c_2 \in [0, 1], \quad (47c)$$

$$c_2 \in \mathbb{I}. \quad (47d)$$

After derivations detailed in Appendix B, $O_{k,j}(\mathcal{P}_c)$ can be further expressed as

$$O_{k,j}(\mathcal{P}_c) = \sum_{\mathbf{x}' \neq \mathbf{x}} \sum_{r=1}^{\mathcal{R}} \sum_{p=1}^P \sum_{n=0}^{N-1} (1 - \cos(\psi_n + \theta'_n - \theta_n)). \quad (48)$$

B. Problem Transformation

1) Transformation regarding \mathbf{x}' and \mathbf{x} :

Since $x'_{\text{loc}_p + n}$ and $\overline{x_{\text{loc}_p + n}}$ are M -PSK constellations, ψ_n is denoted as

$$\psi_n = \frac{2\pi k}{M}, k = -(M-1), \dots, -1, 0, 1, \dots, M-1, \quad (49)$$

where each possible value is assigned with equal probability, i.e., ψ_n follows a discrete uniform distribution.

For the case where $\mathbf{x}' \neq \mathbf{x}$, the computation for $O_{k,j}(\mathcal{P}_c)$ can be expressed as

$$\begin{aligned} O_{k,j}^{(\mathbf{x}' \neq \mathbf{x})}(\mathcal{P}_c) &= \sum_{\mathbf{x}' \neq \mathbf{x}} \sum_{r=1}^{\mathcal{R}} \sum_{p=1}^P \sum_{n=0}^{N-1} (-\cos(\psi_n + \theta'_n - \theta_n)) \\ &= \sum_{r=1}^{\mathcal{R}} \sum_{p=1}^P \sum_{n=0}^{N-1} \left(\sum_{k=1-M}^{M-1} \cos\left(\frac{2\pi k}{M} + \theta'_n - \theta_n\right) \right) \\ &= 0. \end{aligned} \quad (50)$$

Therefore, for the original problem (47a), it is sufficient to consider the case of $\mathbf{x}' = \mathbf{x}$. In this case, $\psi_n = 0$ for all $n = 0, 1, \dots, N$, and $O_{k,j}(\mathcal{P}_c)$ can be obtained as

$$O_{k,j}(\mathcal{P}_c) = \sum_{r=1}^{\mathcal{R}} \sum_{p=1}^P \sum_{n=0}^{N-1} (1 - \cos(\theta'_n - \theta_n)). \quad (51)$$

Then, problem (47a) can be expressed as

$$\max_{\mathcal{P}_c} \min_{k,j \in [1, 2^{b_2}]} \sum_{r=1}^{\mathcal{R}} \sum_{p=1}^P \sum_{n=0}^{N-1} (1 - \cos(\theta'_n - \theta_n)) \quad (52a)$$

$$\text{s.t. } (47b)(47c)(47d). \quad (52b)$$

2) Transformation regarding $\text{P}_{c_2}^{(j)}$ and $\text{P}_{c_2}^{(k)}$:

In problem (52a), each pair of indices of PCPGs, i.e., each pair of j, k , corresponds to a specific set of $P_{c_2}^{(j)}$ and $P_{c_2}^{(k)}$. By substituting (74) into (52a), $O_{k,j}(\mathcal{P}_c)$ can be obtained as

$$O_{k,j}(\mathcal{P}_c) = \sum_{r=1}^{\mathcal{R}} \sum_{p=1}^P \sum_{n=0}^{N-1} (1 - O'), \quad (53)$$

where

$$\begin{cases} O' = \cos\left(2\pi\left(\Delta c_{2,\log_p+n}(\log_p+n)^2 - \Delta c_{2,n}n^2\right)\right), \\ \Delta c_{2,\log_p+n} = c'_{2,\log_p+n} - c_{2,\log_p+n}, \\ \Delta c_{2,n} = c'_{2,n} - c_{2,n}. \end{cases} \quad (54)$$

It can be observed that in the case of $j \neq k$, i.e., $P_{c_2}^{(j)} \neq P_{c_2}^{(k)}$, as the discrepancy between $P_{c_2}^{(j)}$ and $P_{c_2}^{(k)}$ diminishes, the number of zero values in the O' increases. Therefore, in problem (52a), it is sufficient to consider the case where $\|P_{c_2}^{(j)} - P_{c_2}^{(k)}\|_0 = 2$. Hence, the optimization problem can be further expressed as

$$\max_{\mathcal{P}_c} \min_{k,j} \sum_{r=1}^{\mathcal{R}} \sum_{p=1}^P \sum_{n=0}^{N-1} (1 - \cos(\theta'_n - \theta_n)) \quad (55a)$$

$$\text{s.t. } j \neq k, \quad (55b)$$

$$\|P_{c_2}^{(j)} - P_{c_2}^{(k)}\|_0 = 2, \quad (55c)$$

$$c_2 \in (0, 1), \quad (55d)$$

$$c_2 \in \mathbb{I}. \quad (55e)$$

C. Problem Solving

Problem (55) is a non-convex problem, which makes it challenging to obtain a global optimal solution. To this end, the PSO-based algorithm is invoked to obtain a suboptimal solution, attributed to its rapid convergence and exemplary global searching capabilities.

First, a group of N_p particles with velocities and positions are initialized. The velocities of the particles are represented by $\mathcal{V}^{(0)} = \{\mathbf{v}_1^{(0)}, \mathbf{v}_2^{(0)}, \dots, \mathbf{v}_{N_p}^{(0)}\}$, which is indicative of the extent of change occurring during the iterative process. The positions of the particles are denoted by $\mathcal{P}^{(0)} = \{\mathbf{p}_1^{(0)}, \mathbf{p}_2^{(0)}, \dots, \mathbf{p}_{N_p}^{(0)}\}$, where each position represents a potential solution for the pre-chirp alphabet, i.e.,

$$\mathbf{p}_{n_p}^{(0)} = \mathcal{P}_{c,n_p}^{(0)} = \{c_{2,n_p}^{(0,1)}, c_{2,n_p}^{(0,2)}, \dots, c_{2,n_p}^{(0,\lambda)}\}, \quad (56)$$

where n_p represents the index of the particle. As an initial solution, the first particle $\mathbf{p}_1^{(0)}$ is initialized as a heuristic pre-chirp alphabet, where the numbers in \mathcal{P}_c are evenly distributed within the interval $[0,1]$. The remaining particles are randomly initialized.

Subsequently, the fitness value of each particle is evaluated per the specified utility function. In light of the constraints imposed by (55b) and (55c), a brick wall penalty factor is introduced, and the utility function in the i_{ter} -th iteration is defined as

$$\mathcal{F}_P(\mathbf{p}_{n_p}^{(i_{ter})}) = \begin{cases} \epsilon, & \text{if } \mathbf{p}_{n_p}^{(i_{ter})} \text{ is feasible,} \\ -1, & \text{otherwise,} \end{cases} \quad (57)$$

Algorithm 1 PSO-Based Algorithm for c_2 Numerical Selection

Input: $N, G, \lambda, P, \alpha_{\max}, d_{\max}$

Output: \mathcal{P}_c

- 1: Initialize $i_{ter} = 0$ and N_p particles with positions $\mathcal{P}^{(0)}$ and zero velocities $\mathcal{V}^{(0)}$.
 - 2: Calculate the fitness values of all particles by using (57), $\mathcal{F}_P(\mathbf{p}_{n_p}^{(0)})$, $n_p = 1, 2, \dots, N_p$.
 - 3: Initialize the local optimal position of each particle $\mathbf{p}_{n_p,local} = \mathbf{p}_{n_p}^{(0)}$. Calculate the global optimal position $\mathbf{p}_{global} = \text{argmax}(F_p(\mathbf{p}_{n_p}^{(0)}))$, $n_p = 1, 2, \dots, N_p$.
 - 4: **while** $i_{ter} \leq I_{\max}$ **do**
 - 5: **for** $n_p = 1$ to N_p **do**
 - 6: Update the velocity $\mathbf{v}_{n_p}^{(i_{ter})}$ according to (58).
 - 7: **if** $\mathbf{v}_{n_p}^{(i_{ter})} > \mathbf{v}_{\max}$ **then**
 - 8: $\mathbf{v}_{n_p}^{(i_{ter})} \leftarrow \mathbf{v}_{\max}$
 - 9: **else if** $\mathbf{v}_{n_p}^{(i_{ter})} < \mathbf{v}_{\min}$ **then**
 - 10: $\mathbf{v}_{n_p}^{(i_{ter})} \leftarrow \mathbf{v}_{\min}$
 - 11: **end if**
 - 12: Update the position $\mathbf{p}_{n_p}^{(i_{ter})}$ based on (59).
 - 13: Calculate the fitness value $\mathcal{F}_P(\mathbf{p}_{n_p}^{(i_{ter})})$ according to (29).
 - 14: **if** $\mathcal{F}_P(\mathbf{p}_{n_p}^{(i_{ter})}) > \mathcal{F}_P(\mathbf{p}_{n_p,local})$ **then**
 - 15: $\mathbf{p}_{n_p,local} \leftarrow \mathbf{p}_{n_p}^{(i_{ter})}$
 - 16: **end if**
 - 17: **if** $\mathcal{F}_P(\mathbf{p}_{n_p}^{(i_{ter})}) > \mathcal{F}_P(\mathbf{p}_{global})$ **then**
 - 18: $\mathbf{p}_{global} \leftarrow \mathbf{p}_{n_p}^{(i_{ter})}$
 - 19: **end if**
 - 20: **end for**
 - 21: Update $i_{ter} \leftarrow i_{ter} + 1$.
 - 22: **end while**
 - 23: Obtain the global optimal position $\mathcal{P}_c \leftarrow \mathbf{p}_{global}$.
 - 24: **return** \mathcal{P}_c
-

where $\epsilon = \min_{k,j} O_{k,j}(\mathcal{P}_c)$ and $O_{k,j}(\mathcal{P}_c)$ can be obtained by (53). Afterwards, the particle with the greatest fitness value is considered to be the global optimal position \mathbf{p}_{global} , and the local optimal position $\mathbf{p}_{n_p,local}$ of each particle is initialized as $\mathbf{p}_{n_p}^{(0)}$.

Each particle conveys its local optimal position to other particles during the iteration. The velocity and position of each particle will be updated by

$$\mathbf{v}_{n_p}^{(i_{ter})} = \varpi \mathbf{v}_{n_p}^{(i_{ter}-1)} + r_1 \varrho_{local} (\mathbf{p}_{n_p,local} - \mathbf{p}_{n_p}^{(i_{ter}-1)}) + r_2 \varrho_{global} (\mathbf{p}_{global} - \mathbf{p}_{n_p}^{(i_{ter}-1)}), \quad (58)$$

$$\mathbf{p}_{n_p}^{(i_{ter})} = \mathbf{p}_{n_p}^{(i_{ter}-1)} + \mathbf{v}_{n_p}^{(i_{ter})}, \quad (59)$$

where ϖ represents the inertia weight, ϱ_{global} and ϱ_{local} denote the global and local updating coefficients, respectively, r_1 and r_2 are random parameters within the interval $[0,1]$. The particle velocity is constrained to a range between \mathbf{v}_{\min} and \mathbf{v}_{\max} , termed as velocity constraint. Then, the fitness value for all particles should be evaluated, and the global and local optimal positions will be updated. Repeat the above

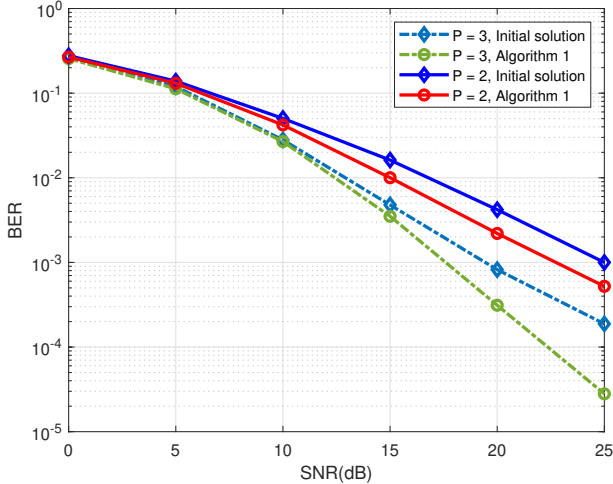


Fig. 4. Performance comparison between Algorithm 1 and initial solution under different parameter settings.

update process until the maximum number I_{\max} of iterations is reached. The particle with the highest fitness value corresponds to the optimization result \mathcal{P}_c . The procedure of the proposed PSO-based algorithm is outlined in Algorithm 1.

VI. SIMULATION RESULTS AND ANALYSIS

In this section, we provide simulation results for the performance evaluation of AFDM-PIM. First, the superiority of the proposed c_2 alphabet design with Algorithm 1 is validated regarding BER performances, where the original alphabet is employed as the benchmark. Then, we conduct the BER performance comparison between the proposed AFDM-PIM scheme and other existing counterparts. Afterwards, the accuracy of the PEP-based theoretical derivation is investigated in comparison with the Monte Carlo simulation results. In simulations, the carrier frequency is set as $f_c = 8$ GHz, and the subsymbol spacing in the DAF domain is set as $f_s = 1.5$ kHz. Two distinct simulation scenarios were conducted, namely when the full diversity condition in (44) is satisfied and not satisfied. Note that the maximum normalized Doppler shifts for these two scenarios are set as $\alpha_{\max} = 1$ and $\alpha_{\max} = 2$, corresponding to the high-speed scenarios with the maximum speed of mobile station of $v_e = 202.5$ km/h and the ultra high-speed scenarios with the maximum speed of mobile station of $v_e = 405$ km/h, respectively. The Doppler shift of each path is generated according to Jakes Doppler spectrum approach as $\alpha_p = \alpha_{\max} \cos(\theta_{p,d})$, where $\theta_{p,d} \in [-\pi, \pi]$ (for integer Doppler cases, the Doppler shift is $\lfloor \alpha_{\max} \cos(\theta_{p,d}) \rfloor$). Besides, we set the pertinent parameters of Algorithm 1 as $\mathbf{v}_{\max} = 0.05$, $\mathbf{v}_{\min} = -0.05$, $q_{\text{global}} = 2$, and $q_{\text{local}} = 2$. Unless otherwise specified, the ML detector is employed for both the proposed AFDM-PIM and the classical benchmarks.

Fig. 4 illustrates the BER performance comparison between Algorithm 1 and the initial solution under the full diversity order condition is satisfied. Binary PSK (BPSK) is employed as the modulation scheme for the data bits. The parameter settings are set as $(N, G, \lambda, d_{\max}, \alpha_{\max}) = (6, 2, 3, 1, 1)$. The

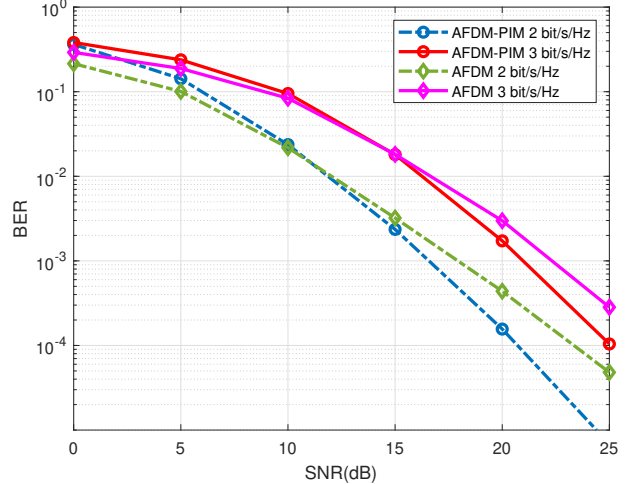


Fig. 5. Performance comparisons between the proposed AFDM-PIM and classical AFDM schemes under different spectral efficiencies.

number of paths is set 2 and 3. As a consequence of satisfying the full diversity order condition, it can be observed that the BER performance of both cases will be improved with the increase in the number of paths. Besides, Fig. 4 shows that Algorithm 1 exhibits superior performance by about 3 dB than the initial solution at the BER level of 10^{-3} . And this enhancement is likely to become more pronounced as the SNR increases.

Fig. 5 compares the BER performance of the proposed AFDM-PIM and classical AFDM [17] schemes under the same doubly dispersive channel, and both of them do not satisfy the full diversity order condition, i.e., the AFDM-PIM does not satisfy the Condition 1 in Theorem 3, while the AFDM does not satisfy the Theorem 1 in [17]. $P = 4$ is assigned for the proposed AFDM-PIM, where BPSK and quadrature PSK (QPSK) are employed to reach the spectral efficiency of 2 and 3 bit/s/Hz, respectively. The other parameters are set as $(N, G, \lambda, d_{\max}, \alpha_{\max}) = (8, 2, 4, 2, 2)$. To reach the same spectral efficiency level in classical AFDM, the number of subcarriers is set as 4, and QPSK and 8-PSK are utilized correspondingly. It can be observed that AFDM-PIM demonstrates a about 2 dB gain compared to the AFDM scheme at the BER level of 10^{-3} , with the gain increasing as the SNR increases. This indicates that AFDM-PIM can provide additional diversity protection and it can be regarded as a viable alternative for communication under a doubly dispersive channel.

In Fig. 6, we evaluate the BER performance of the proposed AFDM-PIM and the AFDM-IM [28] under the spectral efficiencies of 2 and 3 bit/s/Hz. Specifically, $(N, G, \lambda, d_{\max}, \alpha_{\max})$ are set as $(8, 2, 4, 1, 2)$ for AFDM-PIM, and the number of paths is set as $P = 3$. Moreover, the BPSK and QPSK are employed to reach the spectral efficiency of 2 and 3 bit/s/Hz, respectively. In the AFDM-IM scheme, the same doubly dispersive channel is employed, and each group comprises n subcarriers, with a subcarriers activated at each transmission. To reach the same spectral efficiency level in

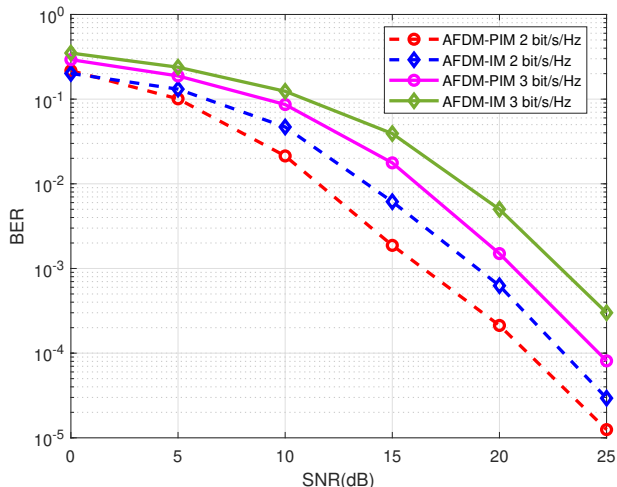


Fig. 6. Performance comparisons between the proposed AFDM-PIM and the AFDM-IM scheme under different spectral efficiencies.

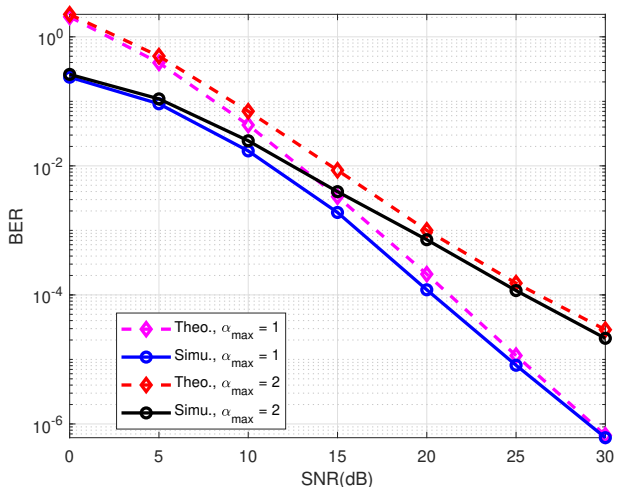


Fig. 7. Comparison of the theoretical ABEP and the simulated BER results of the proposed AFDM-PIM scheme under different Doppler shifts.

AFDM-IM, $(n, a) = (4, 2)$ and $(n, a) = (8, 7)$ are employed, respectively. Note that both of the two schemes do not satisfy the full diversity order condition. One can observe that the AFDM-PIM scheme yields better BER performance than the AFDM-IM scheme about a 2 dB gain at the BER level of 10^{-3} . The enhanced performance is attributable to the stronger diversity protection of the pre-chirp-domain IM.

Fig. 7 presents a comparison of the theoretical ABEP and the simulated BER results of the proposed AFDM-PIM scheme over the doubly dispersive channel. The spectral efficiencies of 1.5 bit/s/Hz are considered, where $(N, G, \lambda, d_{\max})$ are set as $(8, 4, 2, 0)$. The number of paths is set as $P = 3$ and BPSK is employed as the modulation scheme. Besides, the maximum normalized Doppler shifts are set as $\alpha_{\max} = 1$ and $\alpha_{\max} = 2$, corresponding to the high-speed and the ultra high-speed scenarios, respectively. It can be seen that in both cases, the theoretical ABEP results deviate from the

simulated results in the low-SNR region. This is because the PEP calculation is subject to several approximations, which inevitably becomes inaccurate when the noise is dominant. On the other hand, the simulated BER curves present superior consistency with theoretical results at sufficiently high SNRs, which demonstrates the validity of the PEP analysis of AFDM-PIM.

VII. CONCLUSIONS

In this paper, we proposed AFDM-PIM to combat time-frequency doubly selective channel fading. Specifically, the pre-chirp parameters on subcarriers are no longer fixed but are selected from a predefined alphabet. Implicit data transmission is achieved through indexing the specific pre-chirp parameter values on subcarriers, thereby enhancing both spectrum and energy efficiency. The PEP-based theoretical BER upper bounds for the proposed schemes with the ML detection were analyzed and verified through simulations, and the full diversity order conditions of the proposed AFDM-PIM under the doubly dispersive channel were derived. Furthermore, we presented a PSO-based optimization algorithm to design a superior pre-chirp parameter alphabet. Both analytical and simulation results demonstrated that the proposed AFDM-PIM exhibits enhanced spectral efficiency and superior error performance in comparison to classical multi-carrier modulation schemes.

APPENDIX A PROOF OF THEOREM 3

First, we show that Condition 1 is necessary for AFDM-PIM to achieve the full diversity order. For this sake, we assume that the number of paths $P > (d_{\max} + 1)(2\alpha_{\max} + 1)$. Under this assumption, in accordance with the definition of $\text{loc}_p = (\alpha_p + 2Nc_1d_p)_N$, there must be the following situations

$$\exists a, b \in [1, \dots, P], \quad \text{loc}_a = \text{loc}_b. \quad (60)$$

The corresponding two columns in matrix $\Phi(\delta)$ can be written as (61) and (62) on the top of next page, where $\hat{H}_{(\cdot)}[\cdot]\hat{x}$ and $H_{(\cdot)}[\cdot]x$ represents the element in $\hat{\Phi}(\hat{x})$ and $\Phi(x)$, respectively.

Based on (26), the positions of the non-zero entries in matrices $\mathbf{H}_a, \hat{\mathbf{H}}_a, \mathbf{H}_b$ and $\hat{\mathbf{H}}_b$ are consistent. In certain instances, such as when both $\hat{\Phi}(\hat{x})$ and $\Phi(x)$ contain only one single non-zero element at the same position, (61) and (62) are linearly correlated. Therefore, the $\Phi(\delta)$ can not be full rank, i.e., the assumption is not valid.

Besides, when the $\Phi(\delta)$ achieves the full diversity order, the channel paths with different delay values or distinct Doppler frequency shifts are distinguished within the DAFT domain, as shown in Fig. 3, i.e., $(d_{\max} + 1)(2\alpha_{\max} + 1) \leq N$. Therefore, Condition 1 is a necessary prerequisite for achieving the full diversity order.

Then, we prove that Condition 2 can make $\Phi(\delta)$ be full rank. The $\Phi(\delta)$ can be expressed as $\Phi(\delta) = \hat{\Phi}(\hat{x}) - \Phi(x) = [\gamma_1, \dots, \gamma_p, \dots, \gamma_p]$, where γ_p is an N -dimensional column vector with the entries $\gamma_p[n] = \hat{H}_p[n, (\text{loc}_p + n)_N] \hat{x}_{(\text{loc}_p + n)_N} -$

$$\begin{bmatrix} \hat{H}_a[0, \text{loc}_a] \hat{x}_{\text{loc}_a} - H_a[0, \text{loc}_a] x_{\text{loc}_a} \\ \hat{H}_a[1, (\text{loc}_a + 1)_N] \hat{x}_{(\text{loc}_a+1)_N} - H_a[1, (\text{loc}_a + 1)_N] x_{(\text{loc}_a+1)_N} \\ \vdots \\ \hat{H}_a[N-1, (\text{loc}_a + N-1)_N] \hat{x}_{(\text{loc}_a+N-1)_N} - H_a[N-1, (\text{loc}_a + N-1)_N] x_{(\text{loc}_a+N-1)_N} \end{bmatrix}, \quad (61)$$

$$\begin{bmatrix} \hat{H}_b[0, \text{loc}_b] \hat{x}_{\text{loc}_b} - H_b[0, \text{loc}_b] x_{\text{loc}_b} \\ \hat{H}_b[1, (\text{loc}_b + 1)_N] \hat{x}_{(\text{loc}_b+1)_N} - H_b[1, (\text{loc}_b + 1)_N] x_{(\text{loc}_b+1)_N} \\ \vdots \\ \hat{H}_b[N-1, (\text{loc}_b + N-1)_N] \hat{x}_{(\text{loc}_b+N-1)_N} - H_b[N-1, (\text{loc}_b + N-1)_N] x_{(\text{loc}_b+N-1)_N} \end{bmatrix}, \quad (62)$$

$H_p[n, (\text{loc}_p + n)_N] x_{(\text{loc}_p + n)_N}$, $p = 1, 2, \dots, P$, $n = 0, 1, \dots, N-1$.¹

Given constants $\ell_{n,m}$, $\hat{H}_p[n, \text{loc}_p + n]$ can be expressed as $\hat{H}_p[n, \text{loc}_p + n] = \ell_{n,m} H_p[n, \text{loc}_p + n]$. According to (26), the entries of γ_p is given by

$$\begin{aligned} \gamma_p[n] &= H_p[n, \text{loc}_p + n] \rho_{n,m} \\ &= e^{i2\pi[c_{2,\text{loc}_p+n}(\text{loc}_p + n)^2 - c_{2,n}n^2]} \\ &\quad \times e^{i\frac{2\pi}{N}[-(\text{loc}_p + n) + c_1 d_p^2]} \rho_{n,m}, \end{aligned} \quad (63)$$

where $\rho_{n,m} = (x_{\text{loc}_p + n} - \ell_{m,n} \hat{x}_{\text{loc}_p + n})$. It is assumed that a set of numbers β_p that are not all zero that satisfy

$$\sum_{p=1}^P \beta_p \gamma_p = \mathbf{0}. \quad (64)$$

Without loss of generality, the β_b is assumed as the non-zero number, $b \in \{1, 2, \dots, P\}$. The calculation relationship for any n can be obtained as

$$\begin{aligned} &\sum_{p=1}^P \beta_p \gamma_p[n] \\ &= \sum_{p=1}^P \frac{\beta_p}{\beta_b} \gamma_p[n] = 0, \quad \forall n. \end{aligned} \quad (65)$$

From (65), it is not hard to obtain

$$\begin{aligned} \rho_{n,b} &= - \sum_{\substack{p=1 \\ p \neq b}}^P \frac{\beta_p}{\beta_b} \frac{\gamma_p[n]}{H_p[n, \text{loc}_p + n]} \\ &= -e^{-i2\pi c_{2,\text{loc}_b} \text{loc}_b^2} e^{i\frac{2\pi}{N}(Nc_1(-d_b^2 + \text{loc}_b d_b))} \\ &\quad \times \sum_{\substack{p=1 \\ p \neq b}}^P e^{i2\pi[c_{2,\text{loc}_p+n}(\text{loc}_p + n)^2 + c_1 d_p^2 - \frac{\text{loc}_p d_p}{N}]} \frac{\beta_p}{\beta_b} \rho_{n,m}. \end{aligned} \quad (66)$$

Since $\rho_{0,b}$ is a signal error term unrelated to $c_{2,n}$, the phase of $\frac{\beta_p}{\beta_b} (m \neq b)$ must contain $2\pi[c_{2,\text{loc}_b} \text{loc}_b^2 - c_{2,\text{loc}_p+n}(\text{loc}_p + n)^2]$ to eliminate the influence of irrational numbers. On the other hand, if (66) hold, there exists another non-zero β_a ($a \neq b$). Similar to the derivation process of (66), the phase of $\frac{\beta_p}{\beta_a} (m \neq a)$ must contain $2\pi[c_{2,\text{loc}_a} \text{loc}_a^2 - c_{2,\text{loc}_p+n}(\text{loc}_p + n)^2]$. Hence,

¹For the convenience of typesetting, we use $\text{loc}_p + n$ to represent $(\text{loc}_p + n)_N$ throughout the following text.

the calculation relationship of $\frac{\beta_a}{\beta_b}$ and $\frac{\beta_b}{\beta_a}$ can be obtained as $\frac{\beta_a}{\beta_b} \cdot \frac{\beta_b}{\beta_a} = 1$, i.e.,

$$\begin{aligned} &e^{i2\pi c_{2,\text{loc}_b} \text{loc}_b^2} e^{-i2\pi c_{2,\text{loc}_a+n}(\text{loc}_a+n)^2} \\ &\quad \times e^{i2\pi c_{2,\text{loc}_a} \text{loc}_a^2} e^{-i2\pi c_{2,\text{loc}_a+n}(\text{loc}_a+n)^2} \vartheta = 1, \quad \forall n, \end{aligned} \quad (67)$$

where ϑ are complex numbers whose phase do not contain $c_{2,n}$. Given that all of the $c_{2,n}$ are irrational numbers, the phase on the left-hand side of the equation cannot be an integer multiple of 2π . This implies that the imaginary part is not zero so the equation does not hold. Consequently, the initial assumption regarding (64) is invalid, which means that the column vectors of matrix $\Phi(\delta)$ are linearly independent, i.e., the rank of $\Phi(\delta)$ is P . Combining analysis in (43), the AFDM-PIM can achieve the optimal diversity order.

APPENDIX B

DERIVATION PROCESS OF FORMULA $O_{k,j}(\mathcal{P}_c)$

By substituting $\Phi_j^r(\mathbf{x}) = [\mathbf{H}_1 \mathbf{x}, \dots, \mathbf{H}_P \mathbf{x}]$ and $\Phi_k^r(\mathbf{x}') = [\mathbf{H}'_1 \mathbf{x}', \dots, \mathbf{H}'_P \mathbf{x}']$ into $O_{k,j}(\mathcal{P}_c)$ in (47a), the $O_{k,j}(\mathcal{P}_c)$ is further approximated as

$$O_{k,j}(\mathcal{P}_c) = \sum_{\mathbf{x}', \mathbf{x}} \sum_{r=1}^{\mathcal{R}} \sum_{p=1}^P \|\mathbf{H}'_p \mathbf{x}' - \mathbf{H}_p \mathbf{x}\|_2. \quad (68)$$

According to (26), the element of $\mathbf{H}_p \mathbf{x}$ can be expressed as

$$\begin{aligned} \mathbf{H}_p \mathbf{x}(n) &= H_p[n, \text{loc}_p + n] x_{\text{loc}_p + n} \\ &= e^{i2\pi[c_{2,\text{loc}_p+n}(\text{loc}_p + n)^2 - c_{2,n}n^2 d_p]} \\ &\quad \times e^{i\frac{2\pi}{N}[-(\text{loc}_p + n) + c_1 d_p^2]} x_{\text{loc}_p + n}. \end{aligned} \quad (69)$$

Moreover, the element of $\mathbf{H}'_p \mathbf{x}' - \mathbf{H}_p \mathbf{x}$ can be obtained as

$$\begin{aligned} &[\mathbf{H}'_p \mathbf{x}' - \mathbf{H}_p \mathbf{x}](n) \\ &= H'_p[n, \text{loc}_p + n] x'_{\text{loc}_p + n} \\ &\quad - H_p[n, \text{loc}_p + n] x_{\text{loc}_p + n} \\ &= \left(e^{i\frac{2\pi}{N}[Nc'_{2,\text{loc}_p+n}(\text{loc}_p + n)^2 - Nc'_{2,n}n^2]} x'_{\text{loc}_p + n} \right. \\ &\quad \left. - e^{i\frac{2\pi}{N}[Nc_{2,\text{loc}_p+n}(\text{loc}_p + n)^2 - Nc_{2,n}n^2]} x_{\text{loc}_p + n} \right) \\ &\quad \times e^{i\frac{2\pi}{N}(-(\text{loc}_p + n)d_p + Nc_1 d_p^2)}. \end{aligned} \quad (70)$$

Therefore, the norm of $\|\Phi_k^r(\mathbf{x}') - \Phi_j^r(\mathbf{x})\|_F^2$ in (47a) can be calculated as (71).

Based on (74) and the complex calculation formula

$$|a - b|^2 = |a|^2 - 2\Re(a\bar{b}) + |b|^2, \quad (72)$$

$$\begin{aligned} \left\| (\Phi_k^r(\mathbf{x}') - \Phi_j^r(\mathbf{x})) \right\|_F^2 &= \sum_{p=1}^P \sum_{n=1}^N \left| H_p' [n, \text{loc}_p + n] x'_{\text{loc}_p + n} - H_p [n, \text{loc}_p + n] x_{\text{loc}_p + n} \right|^2 \\ &= \sum_{p=1}^P \sum_{n=1}^N \left| e^{i\frac{2\pi}{N} [Nc'_{2,\text{loc}_p + n} (\text{loc}_p + n)^2 - Nc'_{2,n} n^2]} x'_{\text{loc}_p + n} - e^{i\frac{2\pi}{N} [Nc_{2,\text{loc}_p + n} (\text{loc}_p + n)^2 - Nc_{2,n} n^2]} x_{\text{loc}_p + n} \right|^2. \end{aligned} \quad (71)$$

where a, b represent complex number, (71) can be further derived as

$$\begin{aligned} &\left\| (\Phi_k^r(\mathbf{x}') - \Phi_j^r(\mathbf{x})) \right\|_F^2 \\ &= \sum_{p=1}^P \sum_{n=1}^N \left| e^{i\theta'_n} x'_{\text{loc}_p + n} - e^{i\theta_n} x_{\text{loc}_p + n} \right|^2 \\ &= \sum_{p=1}^P \sum_{n=1}^N \left| x'_{\text{loc}_p + n} \right|^2 \\ &\quad - 2\Re \left(x'_{\text{loc}_p + n} \overline{x_{\text{loc}_p + n}} e^{i(\theta'_n - \theta_n)} \right) + \left| x_{\text{loc}_p + n} \right|^2 \\ &= \sum_{p=1}^P \sum_{n=1}^N 2 \left(1 - \Re \left(x'_{\text{loc}_p + n} \overline{x_{\text{loc}_p + n}} e^{i(\theta'_n - \theta_n)} \right) \right), \end{aligned} \quad (73)$$

where $x'_{\text{loc}_p + n}$ and $x_{\text{loc}_p + n}$ are the elements in \mathbf{x}' and \mathbf{x} , respectively. Besides, θ'_n and θ_n are given by

$$\begin{cases} \theta_n = 2\pi \left[c_{2,\text{loc}_p + n} (\text{loc}_p + n)^2 - c_{2,n} n^2 \right], \\ \theta'_n = 2\pi \left[c'_{2,\text{loc}_p + n} (\text{loc}_p + n)^2 - c'_{2,n} n^2 \right]. \end{cases} \quad (74)$$

According to Euler's formula, we further simplify the calculation in (73) as

$$\left\| (\Phi_k^r(\mathbf{x}') - \Phi_j^r(\mathbf{x})) \right\|_F^2 = \sum_{p=1}^P \sum_{n=1}^N 1 - \cos(\psi_n + \theta'_n - \theta_n), \quad (75)$$

where $x'_{\text{loc}_p + n} \overline{x_{\text{loc}_p + n}} = e^{j\psi_n}$, and ψ_n represents the phase difference between $x'_{\text{loc}_p + n}$ and $\overline{x_{\text{loc}_p + n}}$. By substituting (75) into (46), $O_{k,j}(\mathcal{P}_c)$ can be formulated as (48).

REFERENCES

- [1] G. Liu, T. Mao, R. Liu, and Z. Xiao, "Pre-chirp-domain index modulation for affine frequency division multiplexing," in *Proc. Int. Wireless Commun. Mobile Comput. (IWCMC)*, Ayia Napa, Cyprus, May 2024, pp. 0473–0478.
- [2] R. Liu, H. Lin, H. Lee, F. Chaves, H. Lim, and J. Sköld, "Beginning of the journey toward 6G: Vision and framework," *IEEE Commun. Mag.*, vol. 61, no. 10, pp. 8–9, Oct. 2023.
- [3] C.-X. Wang, X. You, X. Gao, X. Zhu, Z. Li, C. Zhang, H. Wang, Y. Huang, Y. Chen, H. Haas, J. S. Thompson, E. G. Larsson, M. D. Renzo, W. Tong, P. Zhu, X. Shen, H. V. Poor, and L. Hanzo, "On the road to 6G: Visions, requirements, key technologies, and testbeds," *IEEE Commun. Surv. Tuts.*, vol. 25, no. 2, pp. 905–974, Feb. 2023.
- [4] D. C. Nguyen, M. Ding, P. N. Pathirana, A. Seneviratne, J. Li, D. Niyato, O. Dobre, and H. V. Poor, "6G internet of things: A comprehensive survey," *IEEE Internet Things J.*, vol. 9, no. 1, pp. 359–383, Jan. 2022.
- [5] J. Shi, J. Hu, Y. Yue, X. Xue, W. Liang, and Z. Li, "Outage probability for OTFS based downlink LEO satellite communication," *IEEE Trans. Veh. Technol.*, vol. 71, no. 3, pp. 3355–3360, Mar. 2022.
- [6] J. Wu and P. Fan, "A survey on high mobility wireless communications: Challenges, opportunities and solutions," *IEEE Access*, vol. 4, pp. 450–476, Jan. 2016.
- [7] R. Hadani, S. Rakib, M. Tsatsanis, A. Monk, A. J. Goldsmith, A. F. Molisch, and R. Calderbank, "Orthogonal time frequency space modulation," in *Proc. IEEE Wireless Commun. Netw. Conf. (WCNC)*, San Francisco, CA, USA, Mar. 2017, pp. 1–6.
- [8] M. Qian, F. Ji, Y. Ge, M. Wen, X. Cheng, and H. V. Poor, "Block-wise index modulation and receiver design for high-mobility OTFS communications," *IEEE Trans. Commun.*, vol. 71, no. 10, pp. 5726–5739, Oct. 2023.
- [9] Z. Wei, W. Yuan, S. Li, J. Yuan, G. Bharatula, R. Hadani, and L. Hanzo, "Orthogonal time-frequency space modulation: A promising next-generation waveform," *IEEE Wireless Commun.*, vol. 28, no. 4, pp. 136–144, Aug. 2021.
- [10] M. S. Omar and X. Ma, "Performance analysis of OCDM for wireless communications," *IEEE Trans. Wireless Commun.*, vol. 20, no. 7, pp. 4032–4043, Jul. 2021.
- [11] B. Wang, Y. Wang, Y. Li, and X. Guan, "Underwater acoustic communications based on ocdm for internet of underwater things," *IEEE Internet Things J.*, vol. 10, no. 24, pp. 22128–22142, Dec. 2023.
- [12] Y. Liu, F. Ji, M. Wen, H. Qing, D. Wan, and Z. Hu, "Message-passing receiver for OCDM in vehicular communications and networks," *IEEE Internet Things J.*, vol. 11, no. 14, pp. 24903–24917, Jul. 2024.
- [13] G. D. Surabhi, R. M. Augustine, and A. Chockalingam, "On the diversity of uncoded OTFS modulation in doubly-dispersive channels," *IEEE Trans. Wireless Commun.*, vol. 18, no. 6, pp. 3049–3063, Jun. 2019.
- [14] W. Shen, L. Dai, J. An, P. Fan, and R. W. Heath, "Channel estimation for orthogonal time frequency space (OTFS) massive MIMO," *IEEE Trans. Signal Process.*, vol. 67, no. 16, pp. 4204–4217, Aug. 2019.
- [15] A. Thomas, K. Deka, P. Raviteja, and S. Sharma, "Convolutional sparse coding based channel estimation for OTFS-SCMA in uplink," *IEEE Trans. Commun.*, vol. 70, no. 8, pp. 5241–5257, Aug. 2022.
- [16] A. Bemani, N. Ksairi, and M. Kountouris, "AFDM: A full diversity next generation waveform for high mobility communications," in *Proc. IEEE Int. Conf. Commun. Workshops (ICC Workshops)*, Montreal, QC, Canada, Jun. 2021, pp. 1–6.
- [17] A. Bemani, N. Ksairi, and M. Kountouris, "Affine frequency division multiplexing for next generation wireless communications," *IEEE Trans. Wireless Commun.*, vol. 22, no. 11, pp. 8214 – 8229, Nov. 2023.
- [18] H. Yin, X. Wei, Y. Tang, and K. Yang, "Diagonally reconstructed channel estimation for MIMO-AFDM with inter-doppler interference in doubly selective channels," *IEEE Trans. Wireless Commun.*, early access, Jun. 2024, doi: [10.1109/TWC.2024.3408458](https://doi.org/10.1109/TWC.2024.3408458).
- [19] Q. Luo, P. Xiao, Z. Liu, Z. Wan, N. Thomos, Z. Gao, and Z. He, "AFDM-SCMA: A promising waveform for massive connectivity over high mobility channels," *IEEE Trans. Wireless Commun.*, early access, Jun. 2024, doi: [10.1109/TWC.2024.3413980](https://doi.org/10.1109/TWC.2024.3413980).
- [20] Y. Ni, Z. Wang, P. Yuan, and Q. Huang, "An AFDM-based integrated sensing and communications," in *Proc. IEEE Int. Symp. Wireless Commun. Sys. (ISWCS)*, Hangzhou, China, Oct. 2022, pp. 1–6.
- [21] T. Mao, Q. Wang, Z. Wang, and S. Chen, "Novel index modulation techniques: A survey," *IEEE Commun. Surv. Tuts.*, vol. 21, no. 1, pp. 315–348, Jul. 2018.
- [22] E. Basar, M. Wen, R. Mesleh, M. Di Renzo, Y. Xiao, and H. Haas, "Index modulation techniques for next-generation wireless networks," *IEEE Access*, vol. 5, pp. 16693–16746, Aug. 2017.
- [23] E. Başar, Ü. Aygözü, E. Panayircı, and H. V. Poor, "Orthogonal frequency division multiplexing with index modulation," *IEEE Trans. Signal Process.*, vol. 61, no. 22, pp. 5536–5549, Nov. 2013.
- [24] T. Mao and Z. Wang, "Terahertz wireless communications with flexible index modulation aided pilot design," *IEEE J. Sel. Areas Commun.*, vol. 39, no. 6, pp. 1651–1662, Jun. 2021.
- [25] M. Wen, B. Zheng, K. J. Kim, M. Di Renzo, T. A. Tsiftsis, K.-C. Chen, and N. Al-Dhahir, "A survey on spatial modulation in emerging wireless systems: Research progresses and applications," *IEEE J. Sel. Areas Commun.*, vol. 37, no. 9, pp. 1949–1972, Jul. 2019.
- [26] P. Yang, M. Di Renzo, Y. Xiao, S. Li, and L. Hanzo, "Design guidelines for spatial modulation," *IEEE Commun. Surv. Tuts.*, vol. 17, no. 1, pp. 6–26, 1st Quart., 2015.
- [27] Y. Tao, M. Wen, Y. Ge, and J. Li, "Affine frequency division multiplexing with index modulation," in *Proc. IEEE Wireless Commun. Netw. Conf. (WCNC)*, Dubai, United Arab Emirates, Apr. 2024, pp. 1–6.

- [28] J. Zhu, Q. Luo, G. Chen, P. Xiao, and L. Xiao, "Design and performance analysis of index modulation empowered AFDM system," *IEEE Wireless Commun. Lett.*, vol. 13, no. 3, pp. 686–690, Mar. 2024.
- [29] P. Raviteja, K. T. Phan, and Y. Hong, "Embedded pilot-aided channel estimation for OTFS in delay–doppler channels," *IEEE Trans. Veh. Technol.*, vol. 68, no. 5, pp. 4906–4917, May 2019.
- [30] M. Chiani and D. Dardari, "Improved exponential bounds and approximation for the Q-function with application to average error probability computation," in *Proc. Global Telecommun. Conf., Bologna, Italy*, Dec. 2002, pp. 1399–1402.
- [31] G. L. Turin, "The characteristic function of hermitian quadratic forms in complex normal variables," *Biometrika*, vol. 47, no. 1-2, pp. 199–201, Jun. 1960.
- [32] M. Wen, E. Basar, Q. Li, B. Zheng, and M. Zhang, "Multiple-mode orthogonal frequency division multiplexing with index modulation," *IEEE Trans. Commun.*, vol. 65, no. 9, pp. 3892–3906, Sep. 2017.